INFN Istituto Nazionale di Fisica Nucleare

ISTITUTO NAZIONALE DI FISICA NUCLEARE

Laboratori Nazionali di Frascati

INFN-13-03/LNF
25th March 2013

Radiation damage: evaluation of cosmic rays fluxes and high intensity radiation beams

D. Di Gioacchino,[1] G. Gatti,[1] L. Ingrosso,[2] A. Marcelli,[1] B.V. Robouch,[1] and B. Spataro[1]

[1]Istituto Nazionale di Fisica Nucleare - Laboratori Nazionali di Frascati, Via E. Fermi 40, I-00044 Frascati, Italy
[2]Istituto Tecnico Industriale Statale "H. Hertz", Via W. Procaccini 70, I-00173 Roma

Abstracts

Cosmic rays causes concern about the lifetime and stability of materials exposed to these radiations and in particular about the life of humans involved in long term missions. Radiations interacting inside a bulk material generate along its track ionization, displacement of atoms through collisions, energy deposition, etc. Calculations to carefully evaluate these effects at low and high energies are important tools to be used in many applications. Indeed, materials and devices exposed to high intensity radiation beams present inside accelerator buildings may experience similar and even higher irradiation phenomena.
We will present and discuss here some calculations of the dose absorbed by reference materials exposed to cosmic radiations. The same tools can be used to evaluate many other phenomena associated to the exposition of intense charged and neutral beams.

*Published by **SIDS–Pubblicazioni***
Laboratori Nazionali di Frascati

Introduction

Beyond the protective layer of the earth atmosphere, the amount of unshielded Cosmic Ray (CR) radiation, both of solar (SCR) and of galactic (GCR) origin is impressive[1,2]. This causes concern about the lifetime of many exposed materials and in particular about the life of humans involved in long term missions, the stability of sensitive devices and also of molecular systems like drugs[3] that could be useful for the survival of humans involved in long term missions or activities in the space stations in the outer space. Materials and devices exposed to high intensity radiation beams in the environments around high-energy rings can experience similar problems and the same procedure used to shield CR can be used to limit the irradiation of materials and devices used in the accelerators.[4]

SW packages for simulations

CR impinging onto a material surface interacts with the bulk target generating along its track ionization, displacement of atoms through collisions, energy deposition, etc. The *specific energy* deposited per unit volume of the target is referred to as the absorbed *dose* [1 Gray (Gy) = J/kg, or 1 rad = 0.01 Gy]. Actually, the ion interaction with the target increases at the end of its trajectory, i.e., at the end of the CR particle range. Beyond the latter, the material is unaffected.

Materials are typically described in terms of their density. However, when the irradiated target is a non-bulk target (e.g., a pharmaceutics product, a drug with excipients or a solution), one has to account for the real density of the active element per cm^3 accounting for the effective dilution and as a consequence, monitor the effects associated to the active element.

For this analysis we used an effective but simpler approach respect to the use of SW packages such as GEANT3 and GEANT-FLUKA that may simulate complex hadron interactions (e.g., protons, He nuclei, mesons, ect.) with a detailed treatment of the electromagnetic interactions and the particle propagation also under a magnetic field. To evaluate irradiation phenomena we also present analytical procedures useful to design and test the efficiency of artificial shields in particular in the low energy range. For the different radiations, the available software tools for the simulations are:

1. 3DMTC-Vinia code[5] with ENDFB6 neutron cross-section data for neutrons;
2. CASINO program[6] for electrons;
3. SRIM program[7] cross-checked by the Bethe equation[8] estimates for protons;
4. SRIM program for cosmic ions;
5. the Bethe equation for mesons.

For the CR reference spectra we used data available from the literature for neutrons[9], electrons[1], protons[1,10] and heavier ions[1], as well as the relative abundance of the CR-ions[11].

To clarify the interaction mechanism, we may start considering the case of a 3 MeV H^+ ion impinging normally onto a MgB_2 surface 90 μm thick, i.e., greater than the penetration range. In Fig.1 we show the penetration and in Fig.2 the displacements induced by collisions.

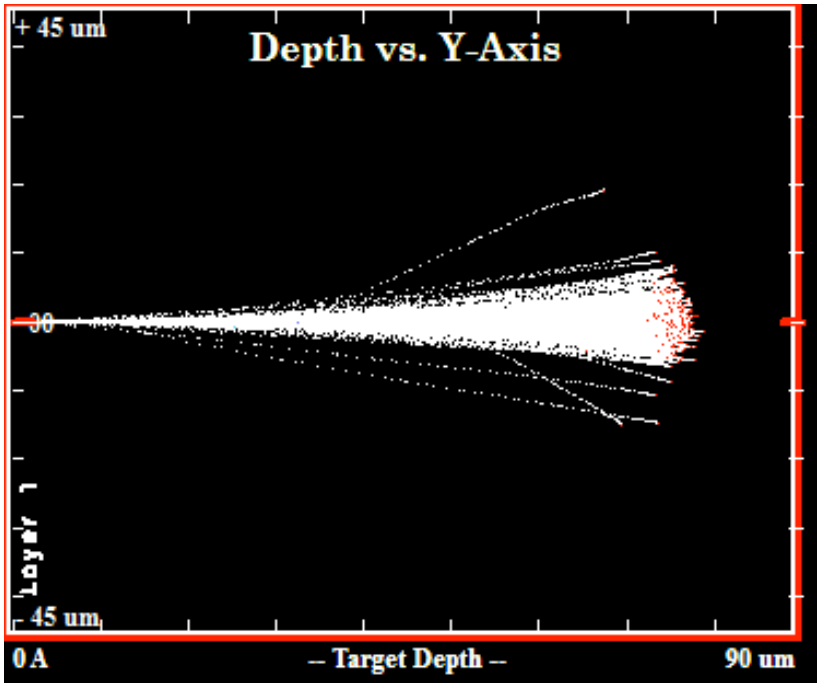

Fig.1: The pattern in one projection plane: x-axis (layer surface) and y-axis (target depth) of a 3 MeV H^+ beam penetrating inside a MgB_2 target ~90 μm thick.

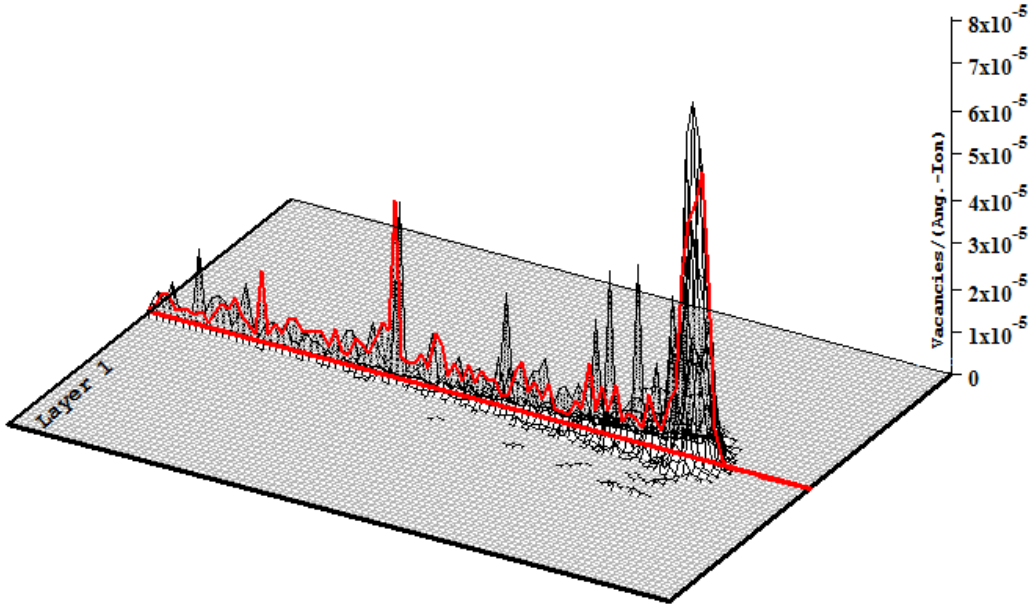

Fig.2: 3D-plot vs. the x-y plane of the penetration of a 3 MeV H^+ beam in a MgB_2 target ~90 μm thick (see Fig. 1). The z-axis shows the number of displacements\vacancies per 3 MeV H^+ ions.

The main goal is to make available a simply tool to design a reliable shield able also to return a first evaluation of the dose absorbed by a material or a target.[1] Because the calculated values are given per incident ion, taking into account the ion-spectrum intensities, the dose absorbed will be the integral over the full ion spectrum.

[1] *N.B.* the energy deposited (E_{dep}) is usually given in [eV/Å ion] to which corresponds the dose [μrad/ion] = 1.6∗E_{dep}/density (g/cm^3).

As an example, in the next we will discuss the evaluation of the dose deposited in a superconductor sample exposed to the Φ-meson DAΦNE flux. This evaluation could be eventually compared with experimental values using a proper setup at DAΦNE (see in the next).

1. Materials exposed to irradiation

To test the simulation of irradiation processes we investigated four elemental metals: Ag, Au, Cu and Pb and a set of five CR particles: H^+, He^+, C^+, Si^+, Fe^+. Calculations clearly show that among the four metals, gold has the highest stopping power (Fig.3). The remaining three: silver, copper and lead are closely grouped although cost and weight considerations would favor the choice of Cu as possible material to shield CR radiation.

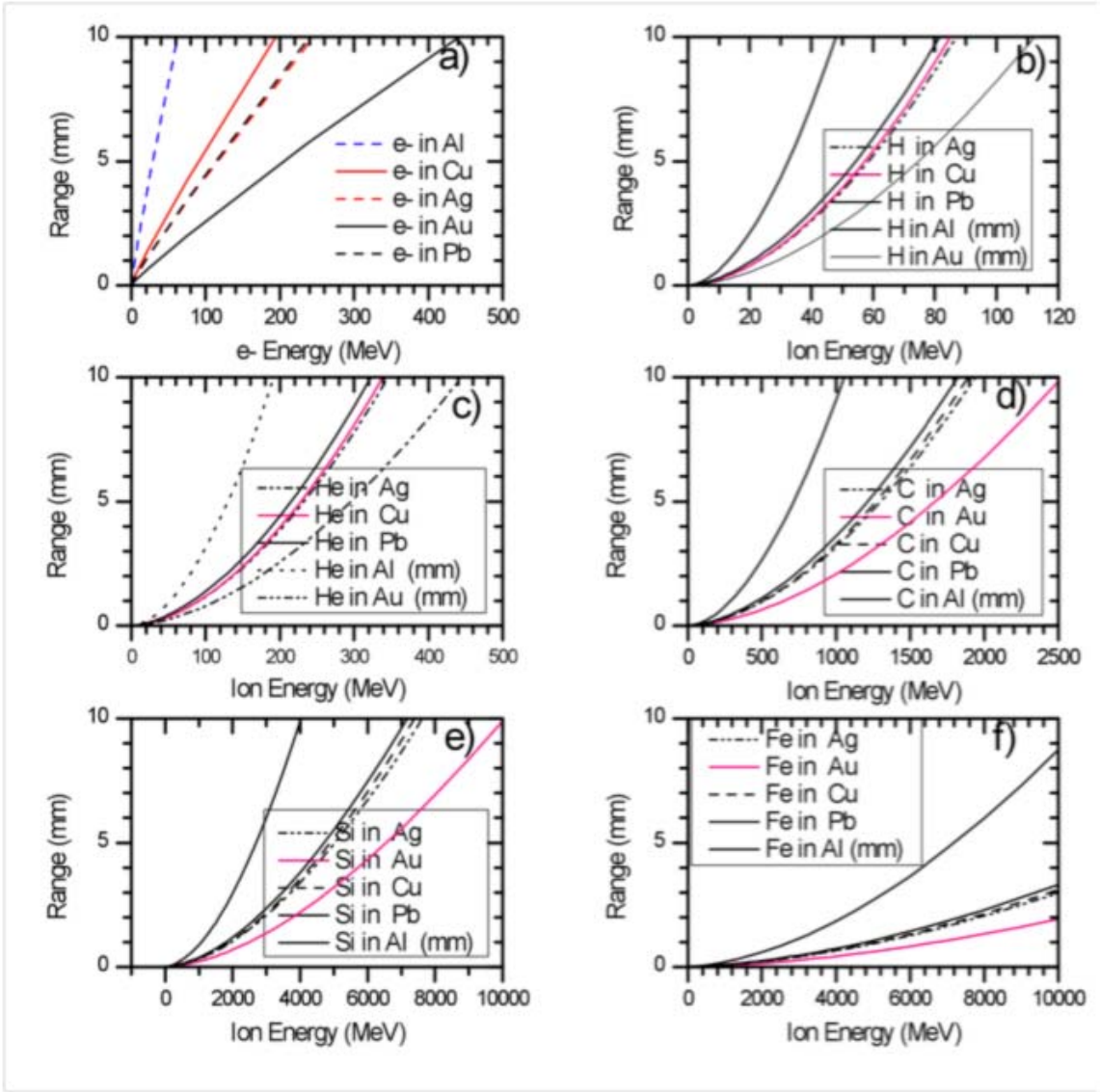

Fig.3: Range (mm) vs. CR incident kinetic energy for H^+, He^+, C^+, Si^+, Fe^+ ions and for Ag, Au, Cu and Pb metals. In the right -bottom graph we compare the stopping power of Au (solid) and Cu (dash).

From data in Fig. 3 we may obtain the maximum energy (MeV) to which a one cm slab of each of the metallic shields stops CR particles: e^-, H, He, C, Si, Fe. (Table-1).

Table-1: Maximum energy (MeV) stopped by one cm metallic shield vs. CR particles

CR-particle [MeV]	shield material Al	Cu	Ag	Au	Pb
e-	60	200	240	440	240
H	50	85	87	110	81
He	190	339	346	440	323
C	1000	1890	1940	2500	1940
Si	4000	7380	7620	10000	7170
Fe	>10000	>10000	>10000	>10000	>10000

2. Effect of CR on materials properties

Using the SW packages it is useful compare the penetration of H^+ ions vs. energy inside different superconductor materials: (light) MgB_2 and (heavy) $YBa_2Cu_3O_7$, $PrFeAsO_{0.08}F_{0.3}$, $SmFe_{0.92}Co_{0.08}AsO$, $Bi_2Sr_2Cu_3O_{10}$, $Bi_{1.6}Pb_{0.4}Sr_2Ca_2Cu_3O_{10}$ (Fig.4).[4]

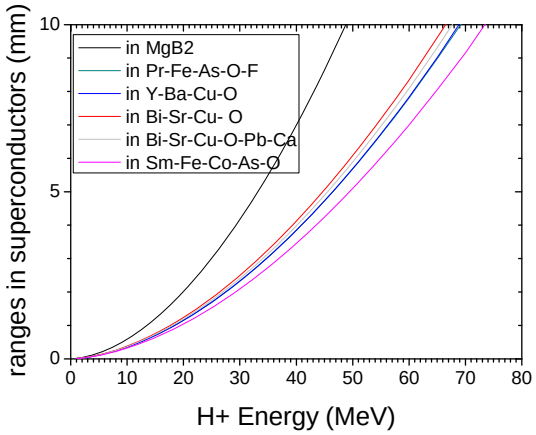

Fig.4: Range (mm) vs. H^+ kinetic energy (MeV/particle) for different superconductors: (light) MgB_2 and (heavy) $YBa_2Cu_3O_7$, $PrFeAsO_{0.08}F_{0.3}$, $SmFe_{0.92}Co_{0.08}AsO$, $Bi_2Sr_2Cu_3O_{10}$, $Bi_{1.6}Pb_{0.4}Sr_2Ca_2Cu_3O_{10}$.

Fig.4 shows that while the superconductor containing mainly low Z atoms (MgB_2) is more transparent than heavier systems: $YBa_2Cu_3O_7$, $PrFeAsO_{0.08}F_{0.3}$, $SmFe_{0.92}Co_{0.08}AsO$, $Bi_2Sr_2Cu_3O_{10}$ and $Bi_{1.6}Pb_{0.4}Sr_2Ca_2Cu_3O_{10}$ that have roughly a similar opaqueness, e.g., H^+ ions of ~50 MeV are totally absorbed in <5 mm by heavier superconductors against ~10 mm of the MgB_2.

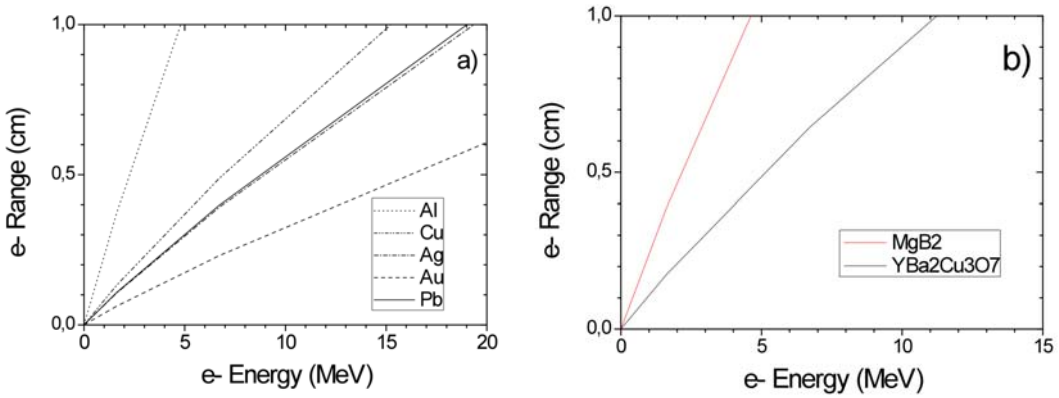

Fig.5 Penetration range of a CR electron flux inside a metallic shield (a) and in two HTS superconductors.

A study of an electron-flux both on a metallic shield and on unshielded superconductors is shown in Fig.s 5 On the left (panel a) we show that a one cm thick slab of Pb or Ag stop electrons accelerated up to 19 MeV and both Al and Cu are less efficient shielding materials compared to gold.

It is extremely interesting to evaluate the damage induced by the exposure of superconductor materials to meson beams, e.g., kaons or pions available at the DAFNE facility where they are the result of the f-meson decay. We simulated the exposure of superconductors in order to determine the fraction dE/E[%] of their absorbed energy (see Table-2) using the available f-meson spectrum at DAΦNE.[12] Among all superconductors we considered, the MgB_2 exhibits the lowest absorption of mesons (kaons 0.85%/mm, pions 5.8%/cm) with only the $SrZrO_3$ system being slightly more transparent (kaons 0.80%/mm, pions 5.5%/cm).

Table-2: Transparency of materials exposed to the ϕ-meson-spectrum and to the decay of kaons and pions at DAΦNE. Materials are listed by dE/E[%] (absorbed energy fraction

materials	kaons	/1 mm		pions	/1 cm
	E.loss [MeV]	**dE/E [%]**		**E.loss [MeV]**	**dE/E [%]**
$C_4H_6O_5$	2.19	0.43			
$SrZrO_3$	4.10	0.80		9.41	5.5
MgB_2	4.32	0.85		9.91	5.8
YB_6	5.67	1.1		13.00	7.6
MgO	6.11	1.20		14.00	8.2
Y_2O_3	7.38	1.45		16.90	9.9
$PrFeAsO_{0.7}F_{0.3}$	8.03	1.6		18.40	10.7
NbTi	8.47	1.66		19.40	11.3
$BaZrO_3$	9.06	1.78		20.80	12.1
$Gd_2Zr_2O_7$	9.43	1.85		21.60	12.6
$YBa_2Cu_3O_7$	9.56	1.88		21.90	12.8
CeO_2	10.70	2.09		24.50	14.3
$NdFeAsO_{0.65}F_{0.35}$	10.80	2.1		24.70	14.4
$NdFeAsO_{0.75}F_{0.25}$	10.80	2.1		24.80	14.4
$SmFe_{0.92}Co_{0.08}AsO$	11.20	2.2		25.70	15.0
NbZr	12.30	2.41		28.10	16.4

The same tools can be used for many other calculations/evaluations, such as the investigation of the potential damage to drugs.[3] To illustrate the possible approach we may consider a pellet of a drug shaped as a parallelepiped of 2x2x2 mm in size, irradiated by a 10 MeV H^+ ion beam. The effects produced by the ion beam inside the target (we considered a pellet made by acetylsalicylic acid, i.e., $C_9H_8O_4$ with a density of 1,35g/cm^3), taken into account by simulations (with a statistics limited to 1000 events) are:

a) Energy deposition [μrad/ion] through ionization (Fig.6);
b) Creation of vacancies [$N_{vacancies}$/Å ion] through collisions (Fig.7) and
c) Emission of phonons [$N_{phonons}$/Å H^+] in the interaction with the target (Fig.8)

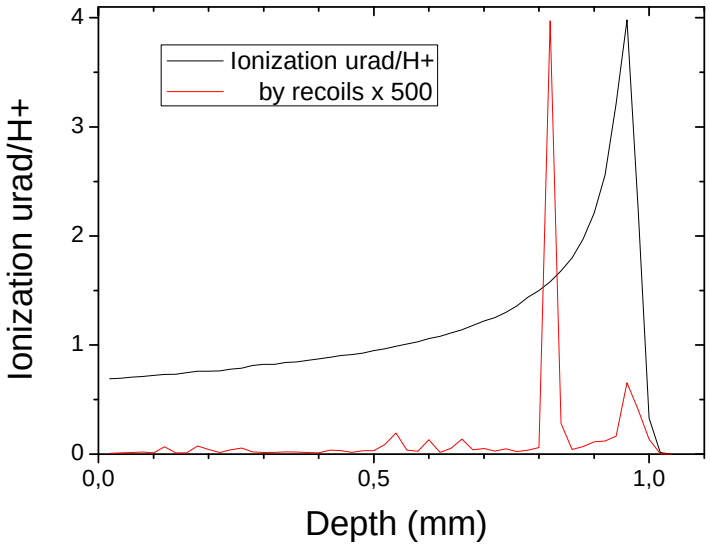

Fig.6: Energy deposited in a pellet through ionizations [µrad/H⁺] by a 10 MeV H⁺ ion beam: directly (black) and by the induced recoil ions (red).

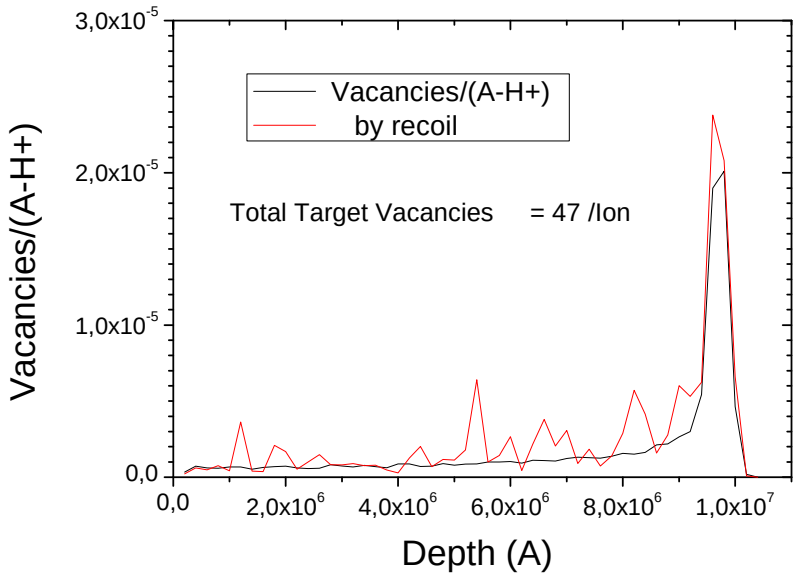

Fig.7: Vacancies produced in a pellet by a 10 MeV H⁺ ion beam directly (black) and through induced-recoil ions (red) 47±7 [$N_{vacancies}$/Å H⁺]

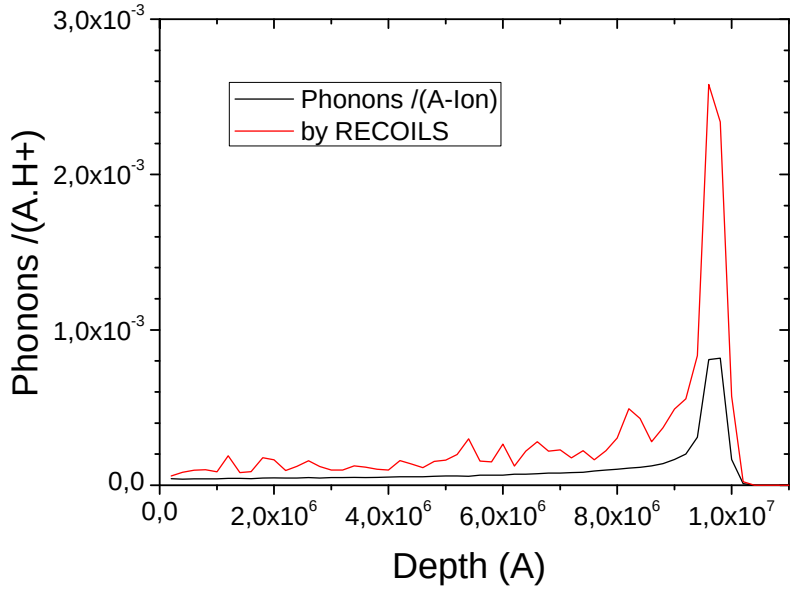

Fig.8: Phonons induced in a pellet by a 10 MeV H⁺ ion beam and recoil ions [$N_{phonons}$/Å H⁺]

To illustrate additional potentialities, we show preliminary results of a Monte Carlo investigation designed to evaluate the possible effects of a flux of kaons, pions and muons using the available production of ϕ-mesons at DAΦNE. In more detail, we reproduced the *Siddharta* layout of which a vertical section perpendicular to the accelerator pipe near the interaction region is shown in Fig.9.

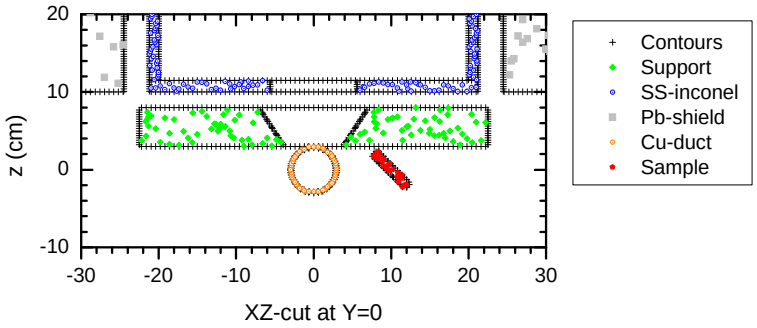

Fig.9 Section of the *Siddharta* layout at DAΦNE used for the computer simulation of the ϕ-meson beam irradiating a planar sample, shown as the red bar in the figure.

In Fig. 9 a superconductor sample is set in the position identified by the red bar. The simulations in Fig. 10 point out that the 1.5 mm thick Cu pipe totally absorbs the kaon flux and only its decaying particles: pions and muons – may reach the sample. Replacing the existing pipe with an equivalent system made in aluminum would allow an appreciable fraction of kaons to hit the sample allowing also to investigate the effects induced by kaons besides those due to other decaying particles. In Fig.10 are represented the distributions (with the relative simulation errors) of the characteristics of kaons from the DAΦNE factory.

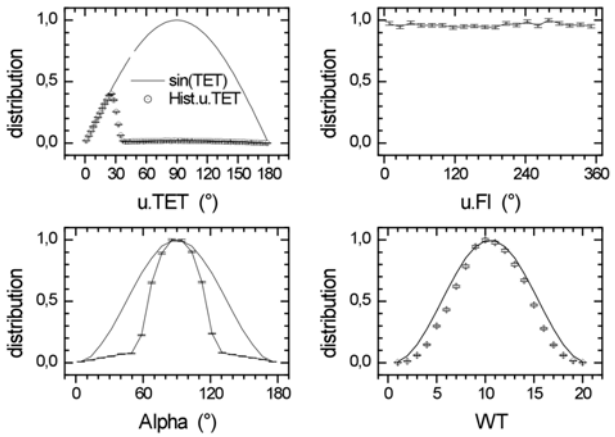

Fig,10 Characteristic distribution of the kaon emission at DAFNE. The homogeneous, anisotropic ($\sin^2\alpha$) emission of the radiation, from left to right, top to bottom: a) & b) velocity components, c) anisotropy effect, d) weight at the emission.

We may show now how is possible to evaluate in a quantitative way the dose released by different radiations in the case of a slab of MgB_2 vs. YBCO exposed to CR (the limit case without the magnetic field on, i.e., without the contribution of the additional physical shield due to the Meissner effect).

3. MgB_2 superconductor exposed to H-ion irradiation

The first example is one cm tick MgB_2 superconductor slab exposed to a H-ion irradiation. The specific damage induced has been calculated considering an energy range from 3 MeV to 10 GeV. Without any shield we observe both displacement of

Mg and B atoms (Fig.11a) and the total dose [mrad/H⁺ion] that the superconductor absorbs vs. the ion energy [MeV] is shown in Fig.11b.

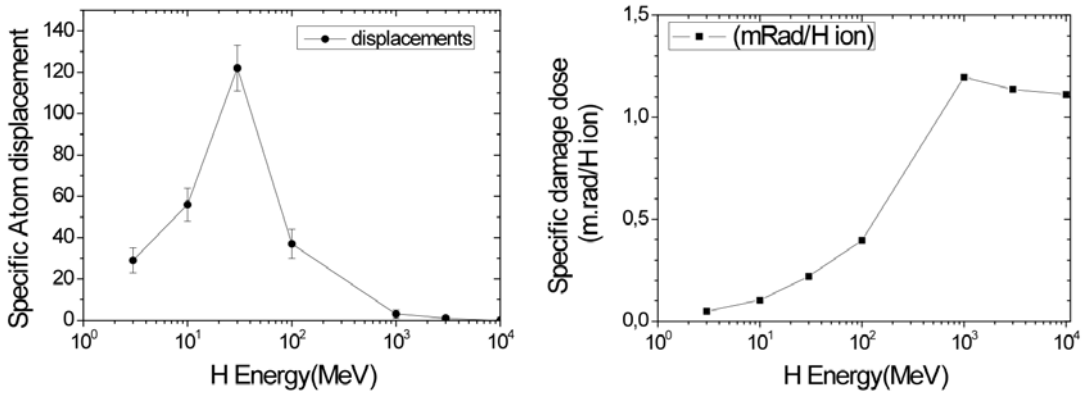

Fig.11 (a) Displacement of MgB_2 atoms vs. H-ion energy; (b) dose absorbed by MgB_2 vs. energy

Actually, as the ion energy raises, the displacement first increases reaching the maximum of 120 atoms at ~ 30 MeV, then rapidly falls once the ion range exceeds the slab thickness of 1 cm at ~49 MeV. Also the dose shown in Fig.11b initially rises reaching a maximum. At higher energies the beam exits the slab and the dose remains almost constant.

Table 3: Calculations of effective shield made by a Cu/MgB_2 slab of 1 cm.

H+ Energy (MeV)	Displacements	Vacancies	Replace Collisions	Range (A)	Ionization (keV/ion)	Phonons (keV/ion)	Damage (keV/ion)	Total E (MeV)
80	653	617	35	89.7	79969.9	28.3	1.85	80
100	502	480	22	186	99973	25.6	1.44	100
1000	33	31	2		999915.3	79.6	5.06	1000
10000	2	2	0		9999940.7	56.8	2.51	10000

If we now consider a double slab composed by one cm of Cu shielding a one cm MgB_2 sample the figures below illustrate its efficiency vs. H^+ ions at different energies: 80 MeV, 100 MeV, 1 GeV and 10 GeV. Lower energy ions do not reach the MgB_2 because ions of 89 MeV have a penetration range of just one cm and stop within copper (Fig.12a). 100 MeV H^+ ions emerge are not fully shielded by Cu (Fig.12b) while 10 GeV H^+ ions cross both Cu and MgB_2 targets and proceed well outside them (Fig.12c).

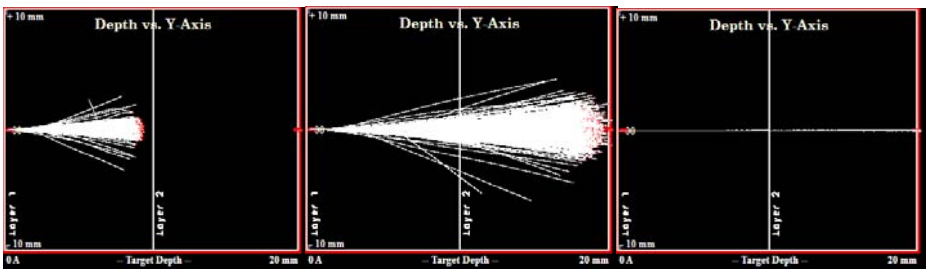

(a) (b) (c)

Fig. 12 Penetration inside the slabs of H^+ ions of 80 MeV (a), 100 MeV (b) and 10 GeV (c).

Many other challenging experimental researches could be associated to these calculations. In particular, at Frascati, we should arrange dedicated setups and perform different kind of experiments to:

- Characterize MgB_2 and YBCO tapes vs. temperature;
- Set irradiation procedures of materials with set-ups specific for the different radiation sources: DAΦNE, BTF, etc;
- Characterize with magnetic and morphological/structural techniques irradiated materials, e.g., superconductors, pharmaceutics, etc.;
- Compare experimental data and simulations for a wide range of applications.

Finally, we show below two examples of cosmic ray spectra of *protons*, *electrons* and *'all-particles'*[1,2] that we used in the above simulations (left and right panels in Fig.13).

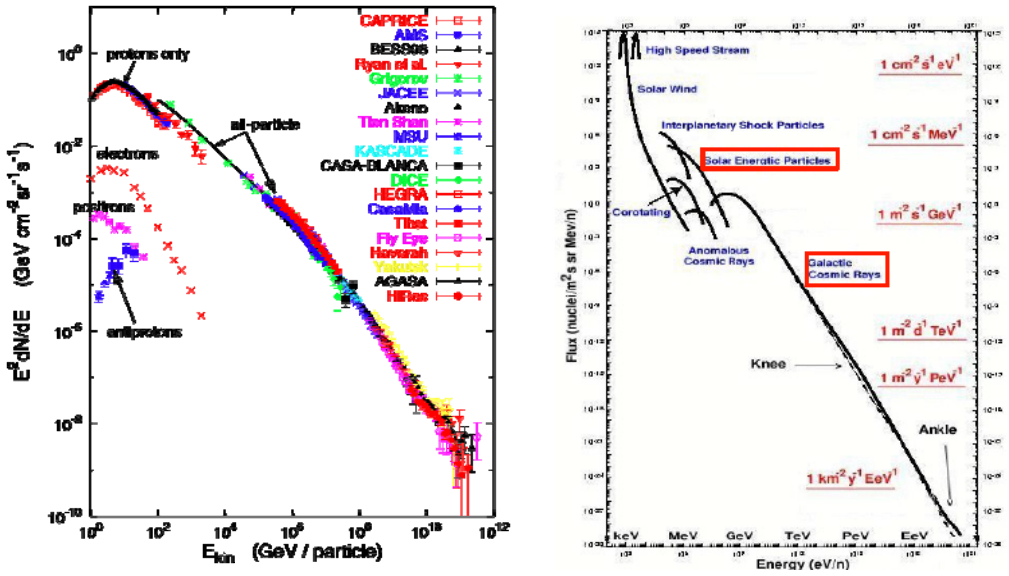

Fig.13: Fluences vs. energy [GeV/particle] of different CR particles[1, 2]

Conclusions

Calculations to carefully evaluate effects induced by intense beam of ionizing radiation at low and high energies are important tools to be used in many applications on the Earth. Actually, the same tools are mandatory to evaluate risks associated to human activities outside the Earth atmosphere. Indeed, although the atmosphere and the geomagnetic field, both significantly reduce the dose associated to the exposition to cosmic radiation, not negligible fluxes of CR are present outside the atmosphere. Here the scenario is substantially different and the dose can easily be at least two orders of magnitude higher. These simulations can be also used to evaluate many other phenomena induced by intense charged and neutral beams as those delivered by accelerator beams. As an example, these tools are also suitable to calculate the amount of vacancies generated in a superconductor material by an intense ion beam or by neutron radiation. Enhancement of performances or damage can be then understood with these simulation techniques.

Acknowledgements

We sincerely acknowledge R. Battiston for many useful discussions in the framework of his project SR2S-RD (Space Radiation Superconducting Shield), an INFN research project funded by CSN5 and connected to the EU FP7 project SR2S (http://magnet.ge.infn.it/sr2s-rd.html).

References

(1) Hillas, A. M., Cosmic Rays: Recent Progress and some Current Questions. *Cosmology, Galaxy Formation and Astroparticle Physics* **2006**.

(2) Burger, W. J. *Summary of the ESA/NASA Studies*; CERN,: Swizerland, 2012; pp 1-60.

(3) Du, B.; Daniels, V. R.; Vaksman, Z.; Boyd, J. L.; Crady, C.; Putcha, L., Evaluation of physical and chemical changes in pharmaceuticals flown on space missions. *The AAPS journal* **2011,** 13, (2), 299-308.

(4) Battiston, R.; Burger, W. J.; Calvelli, V.; Musenich, R.; Choutko, V.; Datskov, V. I.; Della Torre, A.; Venditti, F.; Gargiulo, C.; Laurenti, G.; Lucidi, S.; Harrison, S.; Meinke, R. *Active Radiation Shield for Space Exploration Missions*; INFN: Perugia, Italy, 2012.

(5) Robouch, B. V.; Huebner, K.; Ingrosso, L.; Brzosko, J. S.; Klein, H.; Guldbakke, S., A new approach to fast neutron diagnostic simulation: Monte Carlo with shower and drizzel splitting and finite close-collision treatment. In *International Conference on Monte Carlo Methods for Neutron and Photon Transport Calculations; 25-28 September, Budapest, Hungary*, ed.; Dr. Koblinger, L., Ed. 1990 ; Progress in Nuclear Energy Vol. 24, pp 409-415.

(6) Drouin, D.; Couture, A. R.; Joly, D.; Tastet, X.; Aimez, V.; Gauvin, R., CASINO V2.42: a fast and easy-to-use modeling tool for scanning electron microscopy and microanalysis users. *Scanning* **2007,** 29, (3), 92-101.

(7) Ziegler, J. F.; Biersack, J. P.; Littmark, U., *The Stopping and Range of Ions in Solids*. ed.; Pergamon Press: 1985; p 321.

(8) Bethe, H. A., *Annalen der Physik (Leipzig)* **1930,** 5, 325.

(9) Akopova, A. B.; Manaseryan, M. M.; Melkonyan, A. A.; Tatikyan, S. S.; Potapov, Y., Radiation measurement on the International Space Station. *Radiat. Meas.* **2005,** 39, (2), 225-228.

(10) Reedy, R. C., Elemental and Isotopic Composition of the Galactic Cosmic Rays. *Annu. Rev. Nucl. Part. Sci.* **1983,** 33, 505-537.

(11) Simpson, J. A., Elemental and Isotopic Composition of the Galactic Cosmic Rays. *Annu. Rev. Nucl. Part. Sci.* **1983,** 33, 323-382.

(12) Di Domenico, A., Recent results from KLOE at DAΦNE. Contribution to *5th KEK Topical Conference - Frontiers in Flavor Physics*, ed.; KEK, Ed. Tsukuba, Japan, 2001.